Quaternary Science Reviews 195 (2018) 171–179

Contents lists available at ScienceDirect

Quaternary Science Reviews

journal homepage: www.elsevier.com/locate/quascirev

Refining the Laurentide Ice Sheet at Marine Isotope Stage 3: A data-based approach combining glacial isostatic simulations with a dynamic ice model

T. Pico [a, *], L. Birch [a, b], J. Weisenberg [a], J.X. Mitrovica [a]

[a] Harvard University, Cambridge, MA, United States
[b] Woods Hole Research Center, Falmouth, MA, United States

ARTICLE INFO

Article history:
Received 29 March 2018
Received in revised form
11 July 2018
Accepted 15 July 2018

ABSTRACT

While glacial geologic records track the retreat history of the Laurentide Ice Sheet, constraints on the ice-sheet build-up history are more elusive. As the Laurentide Ice Sheet expanded to its maximum extent at the Last Glacial Maximum (26 ka), it erased most evidence of previous glaciations. However, an increasing number of dated, non-glacial deposits point to a relatively confined Laurentide Ice Sheet during Marine Isotope Stage 3 (MIS 3; 60-26 ka), suggesting rapid ice growth rates leading to the Last Glacial Maximum. In this study we demonstrate that predictions of relative sea-level change due to glacial isostatic adjustment involving a late and rapid growth of the Laurentide Ice Sheet are consistent with sea-level bounds associated non-glacial deposits of MIS 3 age in Canada. We also run a simple dynamic ice model that adopts the paleotopography generated from the glacial isostatic adjustment simulation and show that, using accumulation rates similar to that of the present-day Arctic, rapid glaciation rates starting at mid-MIS 3 (44 ka) are predicted.

1. Introduction

During the last glacial cycle, ice volumes fluctuated considerably leading into the Last Glacial Maximum (LGM, 26 ka; Cutler et al., 2003; Stokes et al., 2012; Lambeck and Chappell, 2001). Yet determining total ice volumes over much of the growth phase is difficult because sea-level rise during the last deglaciation destroyed or submerged the majority of ancient coastlines. The Laurentide Ice Sheet contained the largest excess ice volume at the LGM, expanding over most of Canada and large swaths of the northern United States (Clark and Mix, 2002). Current understanding of the space-time geometry of the Laurentide Ice Sheet build-up is limited by the sparsity of relevant observables that were preserved after the ice sheet reached its maximum extent and most prior ice margin records were erased. Calibration of numerical models aimed at simulating North American glaciation is challenged by this lack of geological constraints (Stokes, 2017). In addition, uncertainties in paleoclimate conditions make it difficult to assign climatic parameters to force these ice sheet models.

A glacial isostatic adjustment (GIA) analysis of anomalously high sea-level markers along the U.S. mid-Atlantic dated to 50-35 ka suggests a late and rapid eastern Laurentide glaciation (Pico et al., 2017), and this is supported by increasingly robust evidence that the Hudson Bay Lowlands were ice-free during this same interval (Dalton et al., 2016). In this study we compare sea-level constraints associated with non-glacial deposits in eastern Canada dated to mid-Marine Isotope Stage (MIS) 3 to gravitationally self-consistent GIA sea-level predictions in order to assess the model of a reduced Laurentide Ice Sheet cover during this time interval. We reconstruct paleotopography using these GIA simulations, which we adopt to prescribe the initial basal topography for a simple numerical ice model. We explore the extent to which assumptions about Earth structure and ice cover during MIS 3 influence predicted ice-growth rates in the final stages of the glaciation phase. The ice model adopts a high-resolution topography starting at mid-MIS 3, and predicts rapid ice growth rates of 3.6×10^{12} m^3/yr, using a maximum mass balance of 0.4 m/yr, which is consistent with attaining LGM ice volumes by 26 ka.

* Corresponding author.
E-mail address: tpico@g.harvard.edu (T. Pico).

https://doi.org/10.1016/j.quascirev.2018.07.023
0277-3791/

2. Background

2.1. Previous ice modeling studies

The evolution of the Laurentide Ice Sheet in the period prior to the LGM is characterized by a sparse record with poor geochronological control (Clark et al., 1993; Kleman et al., 2010). Most dynamic ice models have not been able to capture the rapid growth of ice sheets suggested by global sea-level records (i.e. at inception or MIS 5d; Charbit et al., 2013). The lack of ice margin or ice thickness constraints poses an additional limitation because these represent important boundary conditions for general circulation model (GCM) simulations (Manabe and Broccoli, 1985; Roe, 2001; Beghin et al., 2014; Charbit et al., 2013; Löfverström et al. 2014, 2015). Numerical models for ice evolution are sensitive to topography as well as initial ice conditions, and these are key to determining paleoclimate conditions, as it is well established that the presence of ice sheets impacts atmospheric circulation patterns (Manabe and Broccoli, 1985; Roe, 2001; Beghin et al., 2014; Charbit et al., 2013; Löfverström et al. 2014, 2015).

Despite these limitations, various studies have modeled the evolution of Laurentide Ice Sheet over the glaciation phase. In particular Kleman et al. (2002, 2013) forced a numerical ice sheet model with a spliced GRIP-Vostok temperature record, and inferred the climatological conditions required to predict ice margins consistent with relative ages of glacial landforms, including relict glacial lineations. Stokes et al. (2012) constructed a dynamic thermo-mechanical ice sheet model calibrated to deglacial chronologies, including records of sea-level and glacial isostatic uplift, and ran a simulation over the entire glacial cycle, comparing to geological data when available. The study found that the ice sheet became warm-based during MIS 4 after it grew substantially, and the model was able to capture rapid ice growth during inception, at MIS 5e. These simulations, which incorporated glaciological constraints, predicted an extensive Laurentide Ice Sheet by MIS 3, with ice volumes comparable to (~75% of) LGM conditions, though this period was characterized by several fluctuations in ice extent.

Although the MIS 3 glaciological record is sparse, numerical ice simulations commonly calibrate predictions using $\delta^{18}O$ records from ocean sediment or ice cores (e.g. Charbit et al., 2007). The Laurentide Ice Sheet is assumed to have largely grown to LGM extent by ~40 ka because the majority of oxygen isotope records show values similar to those at LGM by the middle of the glaciation phase during MIS 4 or MIS 3 (i.e., Lisiecki and Raymo, 2005; Shakun et al., 2015; Waelbroeck et al., 2002). However, while benthic $\delta^{18}O$ records are a proxy for global ice volumes, they are characterized by large uncertainties associated with local ocean temperatures or salinity on the order of tens of meters of global mean sea level (Waelbroeck et al., 2002).

2.2. Empirical evidence

Evidence for Laurentide Ice sheet configuration prior to the LGM comprises glacial features and deposits, including till, moraines, glacial striation, and eskers, and non-glacial deposits such as marine, fluvial, or lacustrine successions (Stokes et al., 2015). In addition, glacial flow lines can be determined by analyzing satellite imagery for glacial lineations (Kleman et al., 2010). However these glacial landforms only allow relative age assignments. Ocean sediment cores record meltwater pulses indicating whether ice advanced into certain river drainage basins (Hill et al., 2006; Wickert et al., 2013). Unfortunately, MIS 3 records are typically characterized by poor chronological control given that 40–50 ka reaches the limit of radiocarbon dating. The remaining geological observations are characterized by sparse dates using methods such as optical stimulated luminescence (OSL) or cosmogenic nuclides (Dalton et al., 2016; Briner et al., 2006).

In the Atlantic region of Canada, Dredge & Thorleifson (1987) reported non-glacial deposits containing mastodon remains, peat, and marine shells during the last glacial phase. Remillard et al. (2017) dated these deposits to MIS 3, and these authors concluded that the Magdalen Islands were deglaciated from 60 to 40 ka. Kleman et al. (2010) reported an Atlantic swarm (a group of lineations) that shows restricted extent, but in the absence of absolute dates they concluded these might date to MIS 5. In the St. Lawrence Lowlands there is also evidence of a restricted ice sheet during MIS 3. Clark et al. (1993) described the St. Pierre non-glacial fluvial unit, which is dated to 60-45 ka, and Dionne and Occhietti (1996) dated detrital fragments of unidentified marine shells in the eastern part of this region to 35-31 ^{14}C ka, concluding that the Laurentide Ice Sheet retreated to the southern edge of the Canadian shield at this time. In the central St. Lawrence Lowlands, Parent et al. (2015) dated plant fragments within an alluvial unit to 31.27 ± 0.20 ^{14}C ka and 33.25 ± 0.24 ^{14}C ka (1σ), and reported a marine unit directly overlying these terrestrial deposits, suggesting a later time of marine incursion in the west.

In southern Ontario, organic deposits were dated to 55-40 ^{14}C ka, and Bajc et al. (2015) noted that a vast region of southern Ontario might have been ice free during MIS 3 (Bajc et al., 2015; Mulligan and Bajc, 2017). In the continental U.S. both glacial and non-glacial records exist, including the Roxana silt, a glacial loess with basal sediments estimated to have an age of 55 ka (Curry, 1996; Clark et al., 1993). Hill et al. (2006) observed various meltwater pulses in the Gulf of Mexico from 45 to 28 ka signaling that the Laurentide Ice Sheet had advanced into the Mississippi drainage basin. Carlson et al. (this issue) dated wood in interbedded lacustrine and glacial till to 39.1 ± 0.4 cal ka in central Wisconsin, indicating that this region experienced rapid ice advance that concluded by 30.4 ± 0.9 cal ka. Wood et al. (2010) dated pro-glacial lake sediments in central Indiana to 40-30 ^{14}C ka and concluded that the ice margin was close to the site at that time, despite evidence that the lower peninsula of Michigan was ice free from 46 to 35 cal ka. Colgan et al. (2015) dated lacustrine deposits in southwestern Michigan, and concluded that lower Michigan was ice-free from 65 to 29 ^{14}C ka.

Finally, a site of major importance for Laurentide Ice Sheet configuration during MIS 3 is the Hudson Bay Lowlands (HBL). This region lies between the two major ice domes (Keewatin and Quebec) inferred to exist at LGM, and is therefore a critical location for understanding the shape and volume evolution of the Laurentide Ice Sheet (Kleman et al., 2010; Andrews, 1973). Clark et al. (1993) described the non-glacial Missinaibi formation and freshwater silt in the Nelson River formation, dated to 46-30 ka using thermoluminescence dating, and noted that the HBL was possibly ice free from MIS 5a to MIS 3. Recently Dalton et al. (2016) dated these lacustrine and marine deposits, using both radiocarbon and OSL methods, to MIS 5a and mid-MIS 3, demonstrating that the HBL was likely ice-free during MIS 3, and potentially from MIS 5a through MIS 3, since there is no glacial evidence that remains from this time period. In addition, recent GIA modeling of anomalously high elevation sea-level data from the U.S. mid-Atlantic dated to mid-MIS 3 strongly suggested a reduced eastern Laurentide Ice Sheet at mid-MIS 3 and a rapid growth into the LGM (Pico et al., 2017).

3. Methods

3.1. GIA modeling

We reconstruct paleotopography by running GIA simulations with a prescribed ice loading history. Our calculations are based on the theory and pseudo-spectral algorithm described by Kendall et al. (2005) with a spherical harmonic truncation at degree and order 256. These calculations include the impact of load-induced Earth rotation changes on sea level (Milne & Mitrovica, 1996), evolving shorelines and the migration of grounded, marine-based ice (Johnston, 1993; Milne et al., 1999; Lambeck et al., 2003; Kendall et al., 2005). Our predictions require models for Earth's viscoelastic structure and the history of global ice cover. We adopt the viscosity profile VM2, which is designed to be paired with the ICE-5G ice history (Peltier, 2004). We will explore the sensitivity of our results to plausible variations in the Earth model.

3.2. Initial ice configurations

Previous work shows that dynamic ice models are sensitive to initial topography. We construct a series of initial ice configurations based on geological constraints (Dalton et al., 2016) and GIA modeling (Pico et al., 2017). Each MIS 3 ice configuration belongs to a distinct ice history spanning the entire glacial cycle (120-0 ka). An ice history spanning the entire glacial phase is necessary when predicting GIA-corrected topography, as crustal deformation will depend on the full prior history of ice loading.

The first model we constructed is based on the ICE-5G ice history (Fig. 2A/B; dotted black). In our version of ICE-5G, the ice geometry during the glaciation phase is assumed to be identical to the post-LGM geometry whenever the global mean sea-level values are the same. The remaining model ice histories (ICE-PC2 and ICE-PC3) are modified from ICE-5G to be consistent with results from recent GIA analyses. In particular, following the Pico et al. (2016) analysis of sedimentary core records from the Bohai Sea, peak global mean sea level during MIS 3 is placed at −37.5 m at 44 ka in these model ice histories. Moreover, we also adopt global mean sea-level values of −15 m and −10 m for MIS 5a and 5c, respectively; these values are within bounds (5a: −18 m to 0 m, 5c: −20 m to 1 m) derived by Creveling et al. (2017) on the basis of globally distributed sea level markers from both periods. The global mean sea-level curve for ICE-PC2 and ICE-PC3 is shown in Fig. 2A (blue line).

ICE-PC2 is distinguished from our version of ICE-5G in the following ways: (1) the eastern sector of the Laurentide Ice Sheet is ice-free from 80 to 44 ka; and (2) the ice removed in this exercise, equivalent to 6.8 m of global mean sea level, is distributed uniformly over the western sector of the Laurentide Ice Sheet, and the Cordilleran and Fennoscandian Ice Sheets (Fig. 2C). While a uniform ice thickness in the Cordilleran Ice Sheet is unrealistic, altering its volume has minimal impact on sea level predictions in eastern Canada. Finally, in the ice history ICE-PC3 the eastern sector of the Laurentide Ice Sheet is ice-free (as in ICE-PC2) from 80 to 44 ka except for northern Quebec, which remains glaciated, according to retrodicted patterns of snow accumulation (e.g. Löfverström et al., 2014; See Appendix Fig. 1).

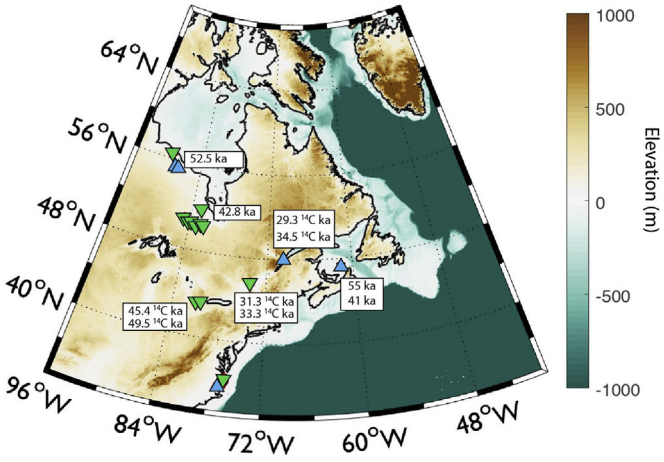

Fig. 1. The location of non-glacial deposits dated to mid-MIS 3 that are discussed in the text. Upward blue triangles denote marine indicators (relative sea-level must be above this elevation) and downward green triangles denote terrestrial indicators (relative sea-level below this elevation). (For interpretation of the references to colour in this figure legend, the reader is referred to the Web version of this article.)

3.3. Ice modeling

We used a simple ice flow model that reduces the three-dimensional Stokes flow equations to two dimensions using the shallow ice approximation (Cuffey and Paterson, 2010) with methodology adopted from Oerlemans (1981) as further developed in Birch et al. (2018). The resulting nonlinear diffusion equation represents ice flow by evolving ice thickness H in time based on the horizontal gradients of the surface elevation H^* and the additional input of the surface mass balance G:

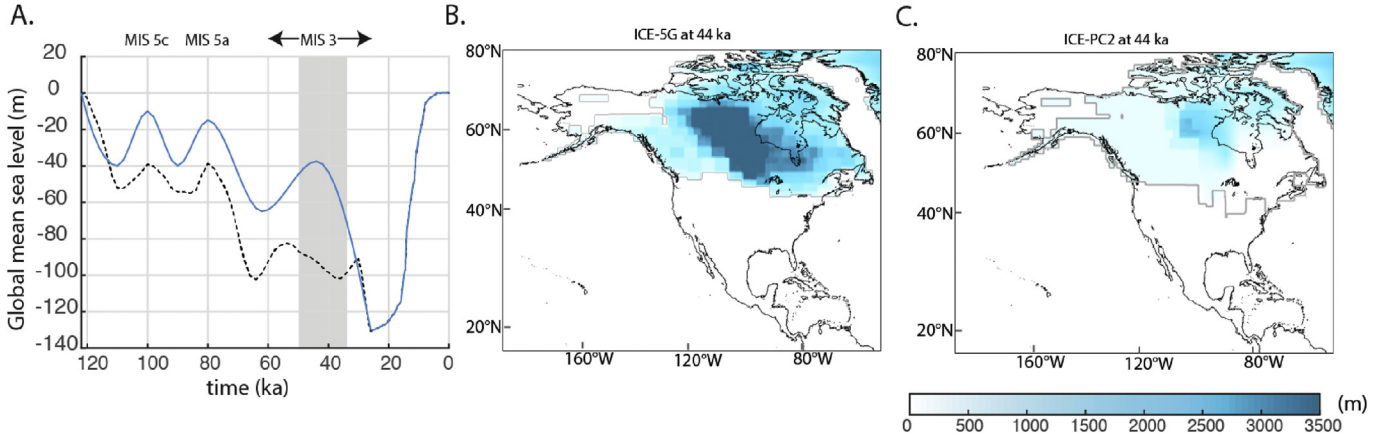

Fig. 2. A. Global mean sea level history for ice history ICE-5G (dotted black) and ICE-PC2 (blue). B. Ice thickness at 44 ka for ice history ICE-5G (B) and ICE-PC2 (C). Maximum ice extent at LGM is shown by gray line in C. (For interpretation of the references to colour in this figure legend, the reader is referred to the Web version of this article.)

$$\frac{\partial H}{\partial t} = \nabla \cdot D \nabla H^* + G$$

The surface elevation (H^*) is defined as

$$H^* = B + H,$$

where B is the basal topography. The non-linear shear thinning of ice flow is represented by diffusivity (D), which depends on both the ice thickness and surface elevation gradients:

$$D = AH^{m+2}\left[\left(\frac{\partial H^*}{\partial x}\right)^2 + \left(\frac{\partial H^*}{\partial y}\right)^2\right]^{(m-1)/2}$$

We adopted a value of $m = 3$ for all model simulations, which is a typical value for realistic ice simulations (Cuffey and Paterson, 2010). The coefficient A, the creep parameter that influences the viscosity of the ice, is based on the temperature of the ice (i.e. colder ice flows more slowly). We adopted a value of $A = 2.4 \times 10^{-24}\,\mathrm{Pa}^{-3}\,\mathrm{s}^{-1}$ based on work by Cuffey and Paterson (2010), where the value of A is based on the temperature at the base of the ice sheet, near the melting point (typical of large ice sheets; Dowdeswell et al., 1997; Cutler et al., 2000; Oerlemans, 2003). The basal sliding velocity is assumed to be zero. The numerical scheme used to integrate this ice model is described in Appendix 2.

The ice model requires that surface elevation (H^*), ice thickness (H), and mass balance (G) be specified as inputs. The ice thickness (H) and surface elevation (H^*) are derived from the initial ice configurations described above (Fig. 2B/C) and the resulting paleotopography changes predicted by GIA simulations adopting the ice histories in Fig. 2A. We specified a grid size of 20 km and a time step of 0.25 yr. We idealized the yearly surface mass balance (G) based on previous studies, where G increases linearly with height until an elevation plateau (Weertman, 1976; Oerlemans, 1989). This upper limit on the mass balance is based on the elevation desert effect, where high elevation ice sheets receive less precipitation (Mahaffy, 1976; Oerlemans, 2003; Birch et al., 2018; Gardner et al., 2011; Dowdeswell et al., 1997). We chose a mass balance slope, which varies as a function of height, of 1 m/yr for every 600 m of elevation gain and a maximum mass balance (net accumulation at high elevation) of 0.4 m/yr for the plateau, according to studies simulating Arctic Canadian glaciers (Dowdeswell et al., 1997; Gardner et al., 2011; Birch et al., 2017).

4. Results

4.1. Predicted topography at MIS 3

We first performed calculations with the ice history ICE-5G. The resulting paleotopography predicted at 44 ka is shown in Fig. 3A. In this case, the simulation predicts that the Hudson Bay Lowlands is largely below sea level, which contradicts terrestrial markers dated to this time interval (Dalton et al., 2016). Moreover, the ice configuration at 44 ka is inconsistent with geological data described above, as ice covers many regions with ice-free markers dated to mid-MIS 3. We next adopted ice history ICE-PC2, characterized by the global mean sea-level history in Fig. 2A (blue line), which has a reduced eastern sector of the Laurentide Ice Sheet until 44 ka (Fig. 2C). The reconstructed topography in the ICE-PC2 simulation predicts that most of Quebec and the Hudson Bay Lowlands are terrestrial, consistent with the majority of the observational data shown in Fig. 1.

4.2. Comparing relative sea-level predictions with empirical data

We next compared the predicted paleotopographies, and associated shorelines, with the geologic constraints on sea level. In particular, we examined data that specifically constrain the relative location of the shoreline with respect to the geologic marker. For example, marine sediments (Fig. 4; upward triangles), including marine species such as molluscs, indicate that the shoreline is above this elevation, while fluvial deposits, peats, or lacustrine sediments are terrestrial indicators (Fig. 4; downward triangles), and demonstrate the shoreline lies below this elevation. To summarize, data from the St. Lawrence River Lowlands record a transition from terrestrial to marine environment at approximately 35 ka (Parent et al., 2015; Dionne and Occhietti, 1996). At the Magdalen Islands marine, terrestrial, and shoreline indicators have been dated from 60 to 40 ka (Remillard et al., 2017). At the Hudson Bay Lowlands recent dates obtained with OSL methods suggest a marine environment to the northwest and terrestrial environment to the southeast. Fig. 5 shows the predicted relative sea level curves from 65 ka to LGM based on the ICE-PC2 ice history at the Hudson

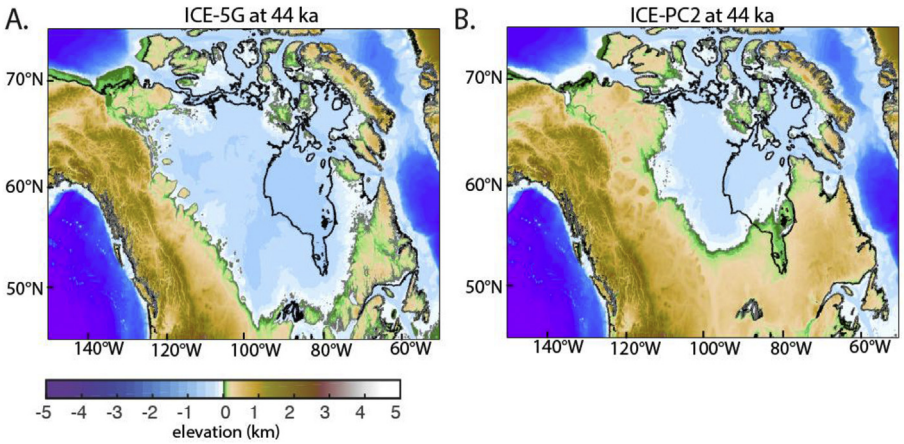

Fig. 3. Predicted paleotopography at mid-MIS 3 (44 ka) using ice history ICE-5G (A) and ICE-PC2 (B).

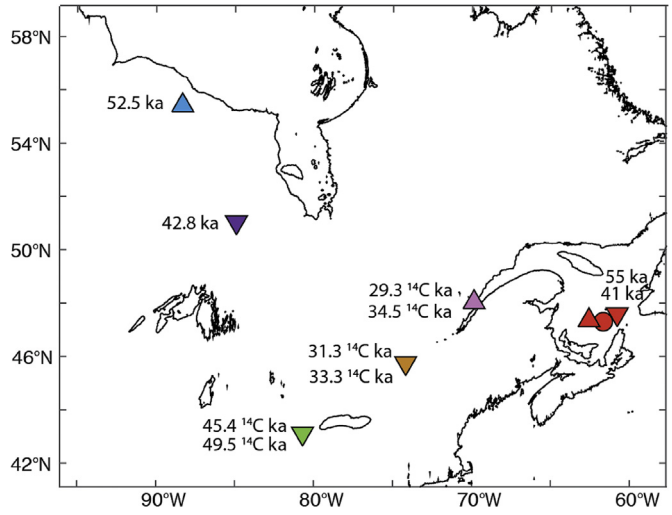

Fig. 4. Location of sea-level markers in eastern Canada. Upward triangles denote marine indicators, downward triangles denote terrestrial indicators. Circles indicate a shoreline marker (data information in Appendix 1). Black lines show present-day shoreline.

Bay Lowlands, the St. Lawrence River Lowlands, Southern Ontario and the Magdalen Islands.

In the HBL we focused on two well-dated sites: 12-PJB-109, a terrestrial marker dated using OSL to 42.8 ± 3.75 ka at 130 m elevation at 50.87° N, 84.85 °W and Severn Marine, a marine sediment dated using OSL to 52.5 ± 5.05 ka (BG3807) and 42.2 ± 4 ka (BG3808), found at 55 m elevation, at 55.43 °N, 88.2 °W (Dalton et al., 2016). We note that at the site 12-PJB-109, we adopt the OSL date since the radiocarbon dates included non-finite ages. Predicted relative sea-level curves for both sites are shown in Fig. 5A. The Severn Marine site (Fig. 5A; blue triangle) is predicted to be 50–150 m higher than present-day sea level, in agreement with the dated marine indicators that place sea level above 55 m from 58 to 38 ka. The terrestrial marker site, 12-PJB-109 (Fig. 5A; purple), is predicted to be below present-day by up to 80 m from 47 to 38 ka, and is not predicted to experience marine flooding until ~40 ka. This is consistent with the elevation of 12-PJB-109 at 130 m, indicating sea level is below this elevation.

At the eastern St. Lawrence Lowlands, predicted relative sea level is lower than present-day (signaling a higher elevation of these markers) until ~35 ka, which is consistent with fluvial deposits dated between 60 and 45 ka (Clark et al., 1993). The predicted marine incursion at ~35 ka agrees with evidence of marine sediments dated to 35-31 ^{14}C ka (Dionne and Occhietti, 1996). The western St. Lawerence Lowlands experiences a delayed sea-level rise relative to the eastern site. Terrestrial markers dated to 33-31 ^{14}C ka (Beta-54140, TO-3990) by Parent et al. (2015) were deposited when sea level is predicted to have risen quickly to submerge this site. The elevation of these markers is ~14 m (Fig. 5B; orange triangle), consistent with the prediction that relative sea level was 0–25 m below present-day sea level at the sites. In Southern Ontario, terrestrial markers were dated to 45.4 ± 1.8 ^{14}C ka (A2392) and 49.5 ± 3.1 ^{14}C ka (A2447) (Mulligan and Bajc, 2017), and at this site relative sea level is predicted to be 25–40 m below present-day from 60 to 40 ka (Fig. 5C; green triangle).

Finally we examined relative sea-level at the Magdalen Islands (Fig. 5C; red circle and triangle) and found that throughout the last glacial cycle from 65 to 26 ka, relative sea-level is predicted to be below present-day, suggesting that there was a terrestrial environment during MIS 3, which is inconsistent with marine deposits dated from 60 to 45 ka (Remillard et al. 2016, 2017). Furthermore, at this site shoreline markers have been dated to 50-35 ka (OSL03, OSL02, OSL55, OSL53, UCIAMS-84792/84793), and this data is similarly inconsistent with GIA predictions that suggest relative sea level at this site was well below this elevation across this time period.

These results indicate that ice history ICE-PC2 produces GIA simulations consistent with geologic records of sea level in the Hudson Bay Lowlands, and St. Lawrence lowlands, but not in the Magdalen Islands, implying that eastern Atlantic sector of the ice loading history may not be accurate.

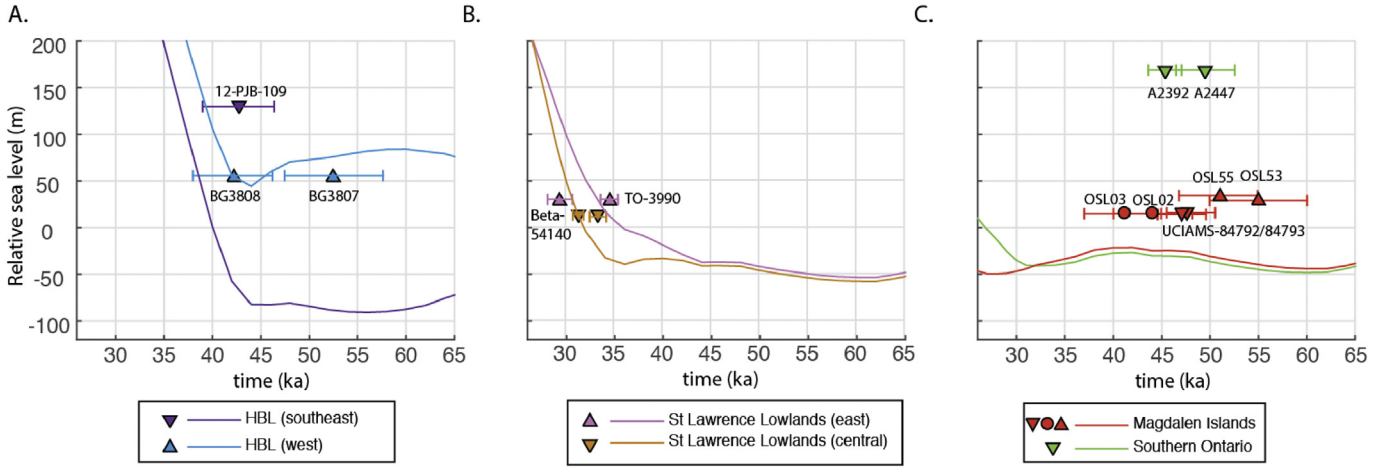

Fig. 5. Relative sea level predictions adopting the ICE-PC2 ice history and VM2 Earth model compared with sea-level markers in A. Hudson Bay Lowlands B. St. Lawrence Lowlands C. Southern Ontario and Magdalen Islands. Upward triangles denote marine indicators, downward triangles denote terrestrial indicators. Circles indicate a shoreline marker (data information in Appendix 1). Location of these markers is shown in Fig. 4. Labels provide identification numbers cited in original publications (as in Table 1). Age uncertainties are reported 1σ errors.

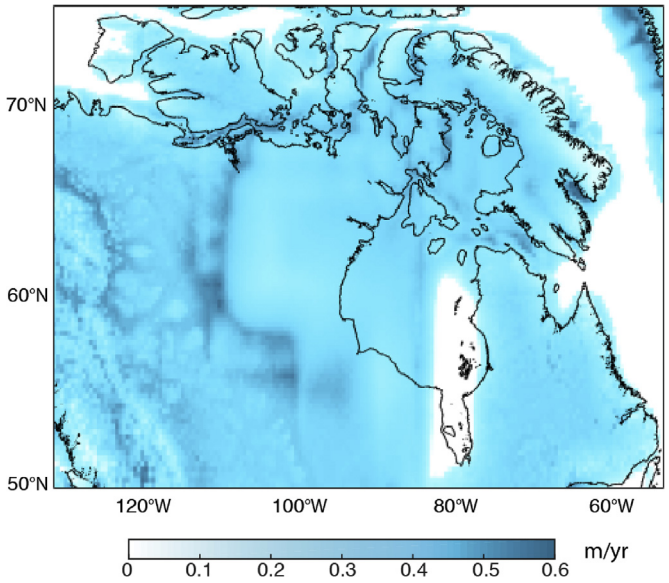

Fig. 6. Ice growth rates averaged over 4.5 kyr using initial ice configuration ICE-PC2 at 44 ka and the paleotopography shown in Fig. 3B.

We conclude by reiterating that these published ages to which we compare our predictions are at the limits of radiocarbon dating, and many of these chronologies include both finite and non-finite ages at the reported site. Alternative dating methods such as OSL are challenged by different uncertainties in age determination. While caution is required in using these dates, the preponderance of MIS 3 ages in these deposits necessitates testing whether GIA-modeling is consistent with the relative sea-level markers associated with these sites.

4.3. Ice growth rates at MIS 3

We ran numerical simulations using the simplified ice flow model described above for 5 kyr to calculate ice growth rates. We initiated the model with the basal topography and ice thickness associated with ice history ICE-PC2 at 44 ka as shown in Fig. 2C and Fig. 3B, respectively, and assign a maximum mass balance (net accumulation at high elevation) of 0.4 m/yr (see Methods and Appendix 2). The resulting rate of ice growth, averaged over a 4.5 kyr period, is shown in Fig. 6. Ice flows rapidly into the unglaciated Hudson Bay Lowlands, and the region over Quebec and Labrador, including the Torngat Mountains, experiences rapid glaciation. Over this 4.5 kyr time period the volume of the Laurentide Ice Sheet more than doubles, growing at a rate of 3.55×10^{12} m^3/yr, and attains a volume of 2.33×10^{16} m^3/yr by 39 ka.

Adopting the basal topography and ice thickness associated with ice history ICE-5G (Figs. 2B and 3A) we predicted an ice volume growth rate of 3.75×10^{12} m^3/yr over the same region (Appendix Fig. 2). A moderately higher rate of ice volume growth is predicted in the ICE-5G case compared to Fig. 5 because ice thickness is greater in the ICE-5G ice history at 44 ka than in ICE-PC2 and therefore in our numerical ice simulations these high elevation regions receive the maximum mass accumulation rate.

To explore the impact of the assumed ice-loading history on predicted ice growth rates, we ran a numerical simulation in which we adopted the basal topography associated with ice history ICE-5G at 44 ka (Fig. 3A), characterized by significant isostatic subsidence under a heavy Laurentide ice load, and paired this with the reduced ice thickness at 44 ka in the ICE-PC2 ice history (Fig. 2C). In this simulation the initial basal topography is at a lower elevation than that associated with ICE-PC2 (Fig. 3B), and therefore the predicted rates of ice volume growth are reduced to 2.46×10^{12} m^3/yr, approximately 70% of the rate predicted using the ICE-PC2 paleotopography (Fig. 3B). Thus, the Laurentide Ice Sheet is predicted to glaciate more slowly, and fewer regions experience rapid, instantaneous glaciation (Appendix Fig. 3).

5. Discussion

5.1. Climate parameters adopted in ice modeling

Climatological conditions are uncertain over much of the last glaciation phase (Charbit et al., 2007; Beghin et al., 2014; Brandefelt & Kjellstr, 2011). We use values for the slope of the mass balance profile and maximum mass balance similar to those adopted in previous studies (Mahaffy, 1976; Pfeffer et al., 1997; Oerlemans, 2003; Cutler et al., 2000; Birch et al., 2018). In numerical simulations using the basal topography and ice thickness associated with ICE-PC2 we varied the slope from 1 m/yr per 300 m to 1 m/yr per 3000 m (a value of 1 m/yr per 600 m was adopted in above simulations). We found that the perturbation to the mass balance slope resulted in similar ice spreading rates, and thus ice volume growth rates are relatively insensitive to this parameter. In contrast, ice volume growth rates are highly sensitive to the value of maximum mass balance; reducing the maximum mass balance by 50% relative to the case considered in Fig. 5 resulted in more than a 50% reduction in ice volume growth rate, yielding a predicted rate of 1.68×10^{12} m^3/yr averaged over a 4.5 kyr period (Appendix Fig. 4).

Precipitation patterns, and therefore the realistic mass balance, likely varied substantially geographically and through time because the growth of large ice sheets alters atmospheric circulation through changes in stationary wave patterns (Roe & Lindzen 2001). However, while it is simplistic to model the variable climatology over the Laurentide Ice Sheet with a single mass balance, we believe that our numerical simulations demonstrate that the predicted ice growth from 44 to 39 ka in the case of a reduced Laurentide Ice Sheet extent (Fig. 2C) is sufficiently rapid to attain LGM ice volumes by 26 ka. We note, in this regard, that the maximum mass balance values adopted here are similar to those calculated at high elevations in the Arctic region at present day (Dowdeswell et al., 1997). In our simulations, we assume that accumulation patterns maintained the Torngat Mountains region in ice-free conditions until 44 ka, but later atmosphere circulation changes caused the region to glaciate rapidly. Nevertheless we explored simulations that initiate with a glaciated Torngat Mountains in ice model ICE-PC3 (Appendix Fig. 5A/B).

To accurately model the evolution of the Laurentide Ice Sheet over the MIS 3 period from 44 ka to 26 ka it will be necessary to realistically simulate changes in climatology associated with a delayed growth during the glaciation phase, an evolution that has previously not been taken into consideration (i.e. Charbit et al., 2007). In particular, the significantly reduced mid-MIS 3 Laurentide Ice Sheet inferred from the non-glacial deposits in Fig. 1 and GIA simulations shown in Fig. 4 may point to a distinct regime of atmospheric circulation across early MIS 3 relative to LGM. In order to explain that the regions containing some of the thickest ice at LGM were ice-free at MIS 3, precipitation patterns must have been quite different than those considered in previous modeling of the

glaciation phase. Furthermore our simulations suggest that the prior history of ice loading during MIS 4 may impact the Laurentide Ice Sheet volume growth rate at MIS 3. Future studies should assess the likelihood of a substantially reduced Laurentide Ice Sheet over much of the glaciation phase from MIS 5a to MIS 3.

5.2. Sensitivity to assumptions of ice thickness and Earth model

Next we assessed the sensitivity of our results to a change in the ice distribution and Earth model adopted in GIA simulations. First we considered the alternate ice history ICE-PC3, characterized by the same global mean sea-level history as ICE-PC2 (Fig. 2A; blue), but distinguished on the basis of the spatial distribution of ice during MIS3. In this ice history, at 44 ka, much of Quebec, including the Torngat Mountains, is glaciated, with an ice-free swatch over the Hudson Bay region. Running our numerical simulations using the basal topography and ice thickness associated with the ICE-PC3 ice history (Appendix Fig. 5A/B) we predicted ice volume growth rates of 3.36×10^{12} m^3/yr, with a total ice volume of 2.33×10^{16} m^3 by 39 ka. These values are negligibly different from the ICE-PC2 based simulation in Fig. 5.

We also tested the sensitivity of our predictions to the choice of Earth model adopted in GIA simulations. We predicted paleotopography at 44 ka using ice history ICE-PC2 and an Earth model characterized by an upper and lower mantle viscosity of 5×10^{20} Pa s and 5×10^{21} Pa s, respectively, and a lithospheric thickness of 48 km (Appendix Fig. 5C and D). The resulting predictions of ice growth indicated that using an alternative Earth model does not impact modeled spreading rates of the ice sheet. In particular, we predict rates of 3.61×10^{12} m^3/yr, with a total ice volume of 2.36×10^{16} m^3 by 39 ka in this case.

A rapid growth of the Laurentide Ice Sheet late in the glacial build-up phase drives a delayed growth of the Laurentide peripheral bulge in GIA simulations, and this could potentially influence estimates of global ice volumes at the LGM. While the majority of sites used to determine global sea level at the LGM (~26 ka) are located in the far-field (i.e. Cutler et al., 2003; Stokes et al., 2012; Lambeck and Chappell, 2001), sites in the intermediate-field of the Laurentide Ice Sheet should be corrected for GIA using an updated MIS 3 ice history prior to considering implications for global ice volumes. For example, we found that at Barbados, a key site used to reconstruct LGM global ice volumes (Peltier & Fairbanks, 2006), GIA simulations adopting the Earth model VM2 and the standard ice history ICE-5G (Peltier & Fairbanks, 2006) predicted that relative sea level is more than 3 m lower at LGM (26 ka) compared to the GIA simulations adopted in Pico et al. (2017), which are based on an ice history characterized by rapid Laurentide Ice Sheet growth. Thus, if we correct the Barbados RSL record for GIA effects with an ice history characterized by a late and rapid Laurentide Ice Sheet, a larger global ice volume (equivalent to ~3 m global mean sea level) would be required to reconcile that record.

6. Conclusion

This study was motivated by recent work suggesting a Laurentide Ice Sheet of limited extent during mid-MIS 3. In particular, we investigate the robustness of the recently proposed Laurentide Ice Sheet configuration by comparing GIA predictions based upon it to RSL bounds implied by non-glacial deposits in the near-field of the Laurentide Ice Sheet. The resulting agreement lends support for arguments of a reduced Laurentide Ice Sheet during MIS 3, and potentially over much of the glaciation phase, implying a rapid growth of the ice sheet leading into the LGM.

Finally, we ran a simple numerical ice simulation to assess whether it is feasible to predict ice growth rates that are consistent with achieving LGM ice volumes in a 15 ky period from mid-MIS 3 to the LGM. We demonstrate, using mass balance values similar to those calculated in the present-day Arctic region, that our numerical ice simulations predict sufficiently rapid ice growth rates at 44 ka during mid-MIS 3 to reconcile the necessary growth towards LGM volumes.

Acknowledgements

We thank C. Stokes and an anonymous reviewer for constructive comments that improved this manuscript. We are grateful to A. Bajc and M. Parent for providing elevation data on published markers dated to MIS 3. This research benefited from insightful discussions with A. Dalton & S. Finkelstein. The authors acknowledge funding from NSF-GRFP (T.P.), NSF Grant EAR-1527351 (J.X.M.), and Harvard University (T.P., J.X.M & J.W.).

Appendix A. Supplementary data

Supplementary data related to this article can be found at https://doi.org/10.1016/j.quascirev.2018.07.023.

Appendix 1

Table 1
Observational data presented in text and Figs. 4 and 5.

Latitude	Longitude	Age (ka)	Age error (kyr) 1σ	Method	Elevation (m)	Indicator	ID/Reference
50.87	84.85	42.8	3.75	OSL	130	terrestrial	12-PJB-109 Dalton et al., 2016
55.43	88.2	52.5	5.05	OSL	55	marine	BG3807 Dalton et al., 2016
55.43	88.2	42.2	4	OSL		marine	BG3808 Dalton et al., 2016
44.28	79.62	45.4	1.8	14C	168.65	fluvial	A2447 Mulligan and Bajc, 2017
44.28	79.62	49.5	3.1	14C	168.65	fluvial	A2392 Mulligan and Bajc, 2017
47.27	61.70	55	5	OSL	30	shallow marine	OSL53 Remillard et al., 2017
47.27	61.70	51	4	OSL	37	beach	OSL55 Remillard et al., 2017
47.22	61.99	47.1	2.3	14C	15	terrestrial	UCIAMS-84792 Remillard et al., 2016
47.22	61.99	47.8	2.5	14C	15	terrestrial	UCIAMS-84793 Remillard et al., 2016
47.22	61.99	41	4	OSL	14.8	beach	OSL03 Remillard et al., 2016
47.22	61.99	44	4	OSL	15.6	beach	OSL04 Remillard et al., 2016
48.10	69.71	29.28	0.68	14C	30	marine	Beta-54140 Dionne and Occhietti, 1996
48.10	69.71	34.51	0.38	14C	30	marine	TO-3990 Dionne and Occhietti, 1996
45.70	74.17	31.27	0.2	14C	14.6	fluvial	Parent et al., 2015
45.70	74.17	33.25	0.24	14C	13.8	fluvial	Parent et al., 2015

Appendix 2. Finite difference approximation

We use the flux form for the finite difference approximation. We use forward Euler and second order centered difference, where n denotes the time step, i the node in the x direction, and j the node in the y direction:

$$\frac{H_{i,j}^{n+1}-H_{i,j}^{n}}{\Delta t}=\frac{D_{i+\frac{1}{2}j}^{n}\left(\frac{H_{i+1,j}^{*n}-H_{i,j}^{*n}}{\Delta x_i}\right)+D_{i-\frac{1}{2}j}^{n}\left(\frac{H_{i,j}^{*n}-H_{i-1,j}^{*n}}{\Delta x_{i-1}}\right)}{\frac{1}{2}(\Delta x_i+\Delta x_{i-1})}+\frac{D_{i,j+\frac{1}{2}}^{n}\left(\frac{H_{i,j+1}^{*n}-H_{i,j}^{*n}}{\Delta y_j}\right)+D_{i,j-\frac{1}{2}}^{n}\left(\frac{H_{i,j}^{*n}-H_{i,j-1}^{*n}}{\Delta y_{j-1}}\right)}{\frac{1}{2}\left(\Delta y_j+\Delta y_{j-1}\right)}+G$$

Next, the numerical expression for the diffusivity is:

$$D_{i+\frac{1}{2},j}^{n}=AH_{i+1/2,j}^{m+2}\left[\left(\frac{H_{i+1,j}^{*}-H_{i,j}^{*}}{\Delta x_i}\right)^2+\left(\frac{1}{2}\left(\frac{H_{i+1,j+1}^{*}-H_{i+1,j-1}^{*}}{\Delta y_{j-1}+\Delta y_j}+\frac{H_{i,j+1}^{*}-H_{i,j-1}^{*}}{\Delta y_{j-1}+\Delta y_j}\right)\right)^2\right]^{(m-1)/2}$$

$$D_{i-\frac{1}{2},j}^{n}=AH_{i-1/2,j}^{m+2}\left[\left(\frac{H_{i,j}^{*}-H_{i-1,j}^{*}}{\Delta x_{i-1}}\right)^2+\left(\frac{1}{2}\left(\frac{H_{i,j+1}^{*}-H_{i,j-1}^{*}}{\Delta y_{j-1}+\Delta y_j}+\frac{H_{i-1,j+1}^{*}-H_{i-1,j-1}^{*}}{\Delta y_{j-1}+\Delta y_j}\right)\right)^2\right]^{(m-1)/2}$$

$$D_{i,j+\frac{1}{2}}^{n}=AH_{i,j+1/2}^{m+2}\left[\left(\frac{H_{i,j+1}^{*}-H_{i,j}^{*}}{\Delta y_j}\right)^2+\left(\frac{1}{2}\left(\frac{H_{i+1,j+1}^{*}-H_{i-1,j+1}^{*}}{\Delta x_{i-1}+\Delta x_i}+\frac{H_{i+1,j}^{*}-H_{i-1,j}^{*}}{\Delta x_{i-1}+\Delta x_i}\right)\right)^2\right]^{(m-1)/2}$$

$$D_{i,j-\frac{1}{2}}^{n}=AH_{i,j-1/2}^{m+2}\left[\left(\frac{H_{i,j}^{*}-H_{i,j-1}^{*}}{\Delta y_{j-1}}\right)^2+\left(\frac{1}{2}\left(\frac{H_{i+1,j+1}^{*}-H_{i-1,j+1}^{*}}{\Delta x_{i-1}+\Delta x_i}+\frac{H_{i+1,j}^{*}-H_{i-1,j}^{*}}{\Delta x_{i-1}+\Delta x_i}\right)\right)^2\right]^{(m-1)/2}$$

Finally, our use of flux form requires the following expressions:

$$H_{i+1/2,j}^{m+2}=\left(\frac{H_{i,j}+H_{i+1,j}}{2}\right)^{m+2}$$

$$H_{i-1/2,j}^{m+2}=\left(\frac{H_{i,j}+H_{i-1,j}}{2}\right)^{m+2}$$

$$H_{i,j+1/2}^{m+2}=\left(\frac{H_{i,j}+H_{i,j+1}}{2}\right)^{m+2}$$

$$H_{i,j-1/2}^{m+2}=\left(\frac{H_{i,j}+H_{i,j-1}}{2}\right)^{m+2}$$

This model uses a 0.25 yr time step. At each time step, a new ice thickness is calculated based on the equations above. Then with the new ice thickness and basal topography known, a new surface elevation is calculated ($H^{*}=B+H$). The edge and center of the ice sheet can lead to a situation in which $D=0$, which is unrealistic behavior. Thus, we set a minimum D; as noted by Oerlemans (1981), and as confirmed in our simulations, the ice model does not depend strongly on this choice.

References

Andrews, J.T., 1973. The Wisconsin Laurentide ice Sheet : dispersal centers, problems of rates of retreat, and climatic implications. Arct. Alp. Res. 5, 185–199.

Bajc, A.F., et al., 2015. Geology and paleoecology of a middle Wisconsin fossil occurrence in Zorra township, southwestern Ontario, Canada. Can. J. Earth Sci. 19 (April), 1–19.

Beghin, P., et al., 2014. Interdependence of the growth of the Northern Hemisphere ice sheets during the last glaciation: the role of atmospheric circulation. Clim. Past 10 (1), 345–358.

Birch, L., Cronin, T., Tziperman, E., 2018. The role of regional feedbacks in glacial inception on Baffin Island : the interaction of ice flow and meteorology. Clim. Past (revised June), 1–28.

Birch, L., Cronin, T., Tziperman, E., 2017. Glacial inception on Baffin Island: the role of insolation, meteorology, and topography. J. Clim. 30 (11), 4047–4064.

Brandefelt, J., Kjellstr, E., 2011. A coupled climate model simulation of Marine Isotope Stage 3 stadial climate. Clim. Past 649–670. https://doi.org/10.5194/cp-7-649-2011 (2010).

Brinessr, J., Gosse, J., Bierman, P.R., 2006. Applications of cosmogenic nuclides to Laurentide Ice Sheet history and dynamics Applications of cosmogenic nuclides to Laurentide Ice Sheet history. Geol. Soc. Am. Spec. Pap. 415, 29–41. https://doi.org/10.1130/2006.2415(03) (October 2014).

Charbit, S., et al., 2007. Numerical reconstructions of the Northern Hemisphere ice sheets through the last glacial-interglacial cycle to cite this version : of the Past Numerical reconstructions of the Northern Hemisphere ice sheets through the last glacial-interglacial cycle. Clim. Past 3, 15–37.

Charbit, S., et al., 2013. The Cryosphere Influence of ablation-related processes in the build-up of simulated Northern Hemisphere ice sheets during the last glacial cycle. Cryosphere 7, 681–698.

Clark, P.U., et al., 1993. Initiation and development of the Laurentide and cordillean

ice sheets following the last interglaciation. Quat. Sci. Rev. 12, 79–114.
Clark, P.U., Mix, A.C., 2002. Ice sheets and sea level of the last glacial maximum. Quat. Sci. Rev. 21, 1–7.
Colgan, P.M., Vanderlip, C.A., Braunschneider, K.N., 2015. Athens Subepisode (Wisconsin Episode) non-glacial and older glacial sediments in the subsurface of southwestern Michigan, USA. Quat. Res. 84, 382–397.
Creveling, J.R., Mitrovica, J.X., Clark, P.U., Waelbroeck, C., Pico, T., 2017. Predicted bounds on peak global mean sea level during marine isotope stages 5a and 5c. Quat. Sci. Rev. 163, 193–208. https://doi.org/10.1016/j.quascirev.2017.03.003. Elsevier Ltd.
Cuffey, K.M., Paterson, W.S.B., 2010. The Physics of Glaciers. Academic Press.
Curry, B.B., 1996. Absence of Glaciation in Illinois during Marine Isotope Stages 3 through 5 Absence of Glaciation in Illinois during Marine (September 2016. https://doi.org/10.1006/qres.1996.0040.
Cutler, K.B., et al., 2003. Rapid sea-level fall and deep-ocean temperature change since the last interglacial period. Earth Planet Sci. Lett. 206 (3–4), 253–271.
Cutler, P.M., et al., 2000. A numerical investigation of ice-lobe-permafrost interaction around the southern Laurentide ice sheet. J. Glaciol. 46 (153), 311–325.
Dalton, A.S., et al., 2016. Constraining the late pleistocene history of the Laurentide ice sheet by dating the Missinaibi formation, Hudson Bay lowlands, Canada. Quat. Sci. Rev. 146, 288–299.
Dionne, J., Occhietti, S., 1996. Apercu du Quaternaiare a L 'Embouchure Du Saguenay, Quebec. Géogr. Phys. Quaternaire 50 (1), 5–34.
Dowdeswell, J.A., et al., 1997. The mass balance of circum-arctic glaciers and recent climate change. Quat. Res. 48 (1), 1–14.
Dredge, L.A., Thorleifson, L.H., 1987. The middle wisconsinan history of the Laurentide ice sheet. Géogr. Phys. Quaternaire 41 (2), 215–235.
Gardner, A.S., et al., 2011. Sharply increased mass loss from glaciers and ice caps in the Canadian Arctic Archipelago. Nature 6–9.
Hill, H.W., et al., 2006. Laurentide Ice Sheet meltwater and abrupt climate change during the last glaciation. Paleoceanography 21, 1–9.
Kendall, R.A., Mitrovica, J.X., Milne, G.A., 2005. On post-glacial sea level - II. Numerical formulation and comparative results on spherically symmetric models. Geophys. J. Int. 161 (3), 679–706. https://doi.org/10.1111/j.1365-246X.2005.02553.x.
Kleman, J., et al., 2010. North American Ice Sheet build-up during the last glacial cycle, 115–21 kyr. Quat. Sci. Rev. 29 (17–18), 2036–2051.
Kleman, J., et al., 2013. Pre-LGM northern hemisphere ice sheet topography. Clim. Past 9 (5), 2365–2378.
Kleman, J., Fastook, J.L., Stroeven, A.P., 2002. Geologically and geomorphologically constrained numerical model of Laurentide Ice Sheet inception and build-up. Quat. Int. (September)
Lambeck, K., Chappell, J., 2001. Sea level change through the last glacial cycle. Science (New York, N.Y.) 292 (5517), 679–686.
Lambeck, K., Purcell, A., Johnston, P., Nakada, M., Yokoyama, Y., 2003. Water-load definition in the glacio-hydro-isostatic sea-level equation. Quat. Sci. Rev. 22 (2–4), 309–318. https://doi.org/10.1016/S0277-3791(02)00142-7.
Lisiecki, L.E., Raymo, M.E., 2005. A Pliocene-Pleistocene stack of 57 globally distributed benthic δ18O records. Paleoceanography 20 (1), 1–17.
Löfverström, M., et al., 2014. Evolution of the large-scale atmospheric circulation in response to changing ice sheets over the last glacial cycle. Clim. Past 10, 1453–1471.
Löfverström, M., Liakka, J., Kleman, J., 2015. the north american cordillera — an impediment to growing the continent-wide Laurentide ice sheet. J. Clim. 28 (2004), 9433–9450.
Mahaffy, M.W., 1976. A three-dimensional numerical model of ice sheets: tests on the barnes ice cap, northwest territories. J. Geophys. Res. 81 (6), 1059–1066. Available at: http://doi.wiley.com/10.1029/JC081i006p01059.
Manabe, S., Broccoli, A.J., 1985. The influence of continental ice sheets on the climate of an ice age. J. Geophys. Res. 90, 2167–2190.
Milne, G. a., Mitrovica, J.X., 1996. Postglacial sea-level change on a rotating Earth: first results from a gravitationally self-consistent sea-level equation. Geophys. J. Int. 126 (3), F13–F20. https://doi.org/10.1111/j.1365-246X.1996.tb04691.x.
Mulligan, R.P., Bajc, A.F., 2017. The pre-Late Wisconsin stratigraphy of southern Simcoe County, Ontario : implications for ice sheet buildup, decay, and Great Lakes drainage evolution 1. Can. J. Earth Sci. 21 (January), 1–21.
Oerlemans, J., 1981. Some basic experiments with a vertically-integrated ice sheet model. Tellus A 33, 1–11. https://doi.org/10.3402/tellusa.v33i1.10690.
Oerlemans, J., 2003. A quasi-analytical ice-sheet model for climate studies to cite this version : nonlinear Processes in Geophysics A quasi-analytical ice-sheet model for climate studies. Nonlinear Process Geophys. 10, 441–452.
Oerlemans, J., 1989. On the response of valley glaciers to climatic change. Glacier Fluctuations and Climatic Change 353–371.
Parent, M., et al., 2015. Mid-wisconsinan fluvial and marine sediments in the central St. Lawrence lowlands - implications for glacial and deglacial events in the appalachian uplands. In: GSA Northeastern Section - 50th Annual Meeting.
Pfeffer, W.T., et al., 1997. Numerical modelling of the late glacial Laurentide advance of ice across Hudson strait:insights into terrestrial and marine geology, mass balance, and calving flux. Paleoceanography 12 (1), 97–110.
Peltier, W.R., Fairbanks, R.G., 2006. Global glacial ice volume and Last Glacial Maximum duration from an extended Barbados sea level record. Quat. Sci. Rev. 25 (23–24), 3322–3337. https://doi.org/10.1016/j.quascirev.2006.04.010.
Pico, T., et al., 2016. Global ice volume during MIS 3 inferred from a sea-level analysis of sedimentary core records in the Yellow River Delta. Quat. Sci. Rev. 152, 72–79.
Pico, T., Creveling, J.R., Mitrovica, J.X., 2017. sea-level records from the U.S. Mid-atlantic constrain Laurentide ice sheet extent during marine isotope stage 3. Nat. Commun. 8 (May), 15612.
Remillard, A., et al., 2017. Relative sea-level changes and glacio-isostatic adjustment on the Magdalen Islands archipelago (Atlantic Canada) from MIS 5 to the late Holocene. Quat. Sci. Rev. 171, 216–233.
Remillard, A.M., et al., 2016. Chronology and stratigraphy of the Magdalen Islands archipelago from the last glaciation to the early Holocene: new insights into the glacial and sea-level history of eastern Canada. Boreas 45 (4), 604–628.
Roe, G., 2001. The mutual interaction between continental-scale ice sheets and atmospheric stationary waves. J. Clim. 14, 1450–1465.
Shakun, J.D., et al., 2015. An 800-kyr record of global surface ocean delta18O and implications for ice volume-temperature coupling. Earth Planet Sci. Lett. 426, 58–68.
Stokes, C.R., 2017. Deglaciation of the Laurentide ice sheet from the last glacial maximum. Cuadernos Invest. Geogr. 43 (2), 377–428.
Stokes, C.R., et al., 2015. On the reconstruction of palaeo-ice sheets : recent advances and future challenges. Quat. Sci. Rev. 125.
Stokes, C.R., Tarasov, L., Dyke, A.S., 2012. Dynamics of the north american ice sheet complex during its inception and build-up to the last glacial maximum. Quat. Sci. Rev. 50, 86–104. Available at: https://doi.org/10.1016/j.quascirev.2012.07.009.
Waelbroeck, C., et al., 2002. Sea-level and deep water temperature changes derived from benthic foraminifera isotopic records. Quat. Sci. Rev. 21 (1–3), 295–305.
Weertman, J., 1976. Milankovitch solar radiation variations and ice age ice sheet sizes. Nature 261 (5555), 17–20.
Wickert, A.D., et al., 2013. Gradual demise of a thin southern Laurentide ice sheet recorded by Mississippi drainage. Nature 502 (7473), 668–671.
Wood, J.R., et al., 2010. Lacustrine sediments in Porter Cave, Central Indiana, USA and possible relation to Laurentide ice sheet marginal positions in the middle and late Wisconsinan. Palaeogeogr. Palaeoclimatol. Palaeoecol. 298 (3–4), 421–431. Available at: https://doi.org/10.1016/j.palaeo.2010.10.033.